STATIC AND DYNAMIC FOLDING OF THREE-DIMENSIONAL ELASTIC MATERIALS

Davide Bigoni[1] and Panos A. Gourgiotis[2]

[1] Department of Civil, Environmental and Mechanical Engineering
University of Trento, Via Mesiano 77 – 38123 Trento, Italy
[2] School of Engineering & Computing Sciences, Durham University, South Road,
Durham, DH1 3LE, U.K.

ABSTRACT

Different from Cauchy elastic materials, generalized continua and in particular constrained Cosserat materials, can be designed to possess extreme orthotropy properties and in this way to model folding and faulting in a three-dimensional solid. Following this approach, folding and faulting spontaneously emerge as a deformation pattern occurring in a strongly anisotropic solid. These patterns are obtained with a perturbation technique, which involves the derivation of new two-dimensional Green's functions for applied concentrated force and moment. The results of the presented study show that extreme materials can be realized in practice and employed to explore, as yet, unattained mechanical behaviors.

1 INTRODUCTION

During folding, bending localizes at sharp edges separated by almost undeformed elements. This mechanical process is uncommon in Nature, although some exceptions can be found in unusual layered rock formations (called 'chevrons') and seashell patterns (for instance Lopha cristagalli). In elasticity, bending is common (for example, in bulk wave propagation), but folding is usually not achieved. The present work shows the route leading to folding for an elastic solid is couple-stress theory with an extreme anisotropy. Materials with extreme mechanical anisotropy are designed to work near a material instability threshold where they display stress channelling and strain localization, effects that can be exploited in several technologies. Material instabilities are analyzed in terms of: positive definiteness of the strain energy, strong ellipticity, wave propagation, ellipticity, and emergence of surfaces of discontinuity [1].

A perturbation technique is introduced to demonstrate folding, which involves the derivation of new Green's functions for applied concentrated force and moment. While the former perturbation reveals folding, the latter shows that a material in an extreme anisotropic state is also prone to a faulting instability, in which a displacement step of finite size emerges [2, 3]. Green's functions are derived for antiplane and plane strain states, for static and time-harmonic forces, which opens the way to integral equations and boundary element techniques.

In dynamics, the Green's function approach shows that the folding which emerges near a steadily pulsating source (in the limit of failure of ellipticity) is transformed into a disturbance with wave fronts parallel to the folding itself. Special attention is devoted to the presence of rotational micro-inertia. This feature is explored as connected to pattern formation. It is shown that its magnitude can change the sign of the lower-order derivatives in the differential equations of motion, so that its effect on the emergence of deformation patterns is very complex and sometimes counter-intuitive [4].

2 FUNDAMENTALS OF CONSTRAINED COUPLE-STRESS ANISOTROPIC ELASTICITY

In this Section, the equations governing the linearized elastic mechanical response are introduced for anisotropic couple-stress solids. A detailed presentation of the three-dimensional theory can be found in [1]. For linear constitutive behavior, the strain-energy density assumes the following general quadratic form for *centrosymmetric* materials

$$W = \frac{1}{2}\mathbb{C}_{pqmn}\varepsilon_{pq}\varepsilon_{mn} + \frac{1}{2}\mathbb{B}_{pqmn}\kappa_{pq}\kappa_{mn}, \tag{1}$$

where $\kappa_{pq} = \omega_{q,p}$ is the curvature tensor defined as the gradient of the rotation $\omega_q = (1/2)e_{qpk}u_{k,p}$ e_{qpk} isthe Levi-Civita alternating symbol, u_q is the displacement vector, ε_{pq} is the standard strain tensor, and $(\mathbb{C}_{pqmn}, \mathbb{B}_{pqmn})$ are the elasticity tensors.

The equations of motion in terms of the displacement components (the counterpart of the Navier-Cauchy equations of the classical theory) assume the following form [4]

$$\mathbb{C}_{pqmn}\partial_m\partial_p u_n - \frac{1}{4}e_{pqk}e_{smn}\mathbb{B}_{rkts}\partial_m\partial_p\partial_r\partial_t u_n - \frac{1}{2}e_{pqk}\partial_p Y_k + X_q = \rho\ddot{u}_q - \frac{\rho\hbar_{ks}^2}{12}e_{pqk}e_{smn}\partial_m\partial_p\ddot{u}_n. \tag{2}$$

in which $\partial_q \equiv \partial(\ )/\partial x_q$, X_q the body force per unit volume, Y_q the body couple per unit volume, $\rho > 0$ is the mass density, and $\hbar_{pq}$ is the micro-inertia structural tensor the components of which have dimensions of [length]. The superposed dot denotes time differentiation and the comma denotes spatial differentiation with respect to rectangular Cartesian coordinates. Indicial notation and the usual summation convention on repeated indices is used throughout the paper.

The necessary and sufficient conditions for the strain energy density W in Eq. (1) to be positive definite (PD) are

$$\mathbb{C}_{pqmn}\varepsilon_{pq}\varepsilon_{mn} > 0, \quad \forall \varepsilon_{pq} \in \text{Sym}\backslash\{0\} \quad \text{and} \quad \mathbb{B}_{pqmn}\kappa_{pq}\kappa_{mn} > 0, \quad \forall \kappa_{pq} \in \text{Dev}\backslash\{0\} \tag{3}$$

where Sym denotes the set of all symmetric tensors, Dev is the set of all deviatoric tensors, and 0 denotes the null element, which is excluded from the definition of positive definiteness. The condition of (PD) is sufficient for unconditional *stability* and *uniqueness* of the solution of the mixed boundary value problem [2,5].

The propagation of plane waves in couple-stress elasticity is now considered. By substituting a plane-wave solution in the equations of motion (2) and assuming null body forces and couples, leads to the propagation condition [4]

$$\left[\mathbb{A} - \rho\omega^2\mathbf{I}\right]\mathbf{M}^{1/2}\mathbf{d} = \mathbf{0}, \tag{4}$$

where $\mathbf{d}$ is the wave amplitude vector, ω is the angular frequency, $\mathbf{I}$ is the identity tensor, $\mathbb{A} = \mathbf{M}^{-1/2}\mathbf{A}\mathbf{M}^{-1/2}$ is the *acoustic tensor* for a constrained Cosserat medium with micro-inertia and $\mathbf{M} = \mathbf{I} + \mathbf{\Gamma}$ with

$$A_{qn}(k,\mathbf{n}) = k^2 A_{qn}^{(\mathbb{C})}(\mathbf{n}) + k^4 A_{qn}^{(\mathbb{B})}(\mathbf{n}), \qquad \Gamma_{qn}(k,\mathbf{n}) = k^2 \frac{\hbar_{qn}^2}{12}e_{pqk}e_{smn}n_m n_p, \tag{5}$$

and

$$A_{qn}^{(\mathbb{C})}(\mathbf{n}) = \mathbb{C}_{pqmn}n_p n_m \quad \text{and} \quad A_{qn}^{(\mathbb{B})}(\mathbf{n}) = \frac{1}{4}e_{pqk}e_{smn}n_m n_p n_l n_r \mathbb{B}_{rkts}, \tag{6}$$

where $\mathbf{n}$ the unit propagation vector, and k the wavenumber (in general complex). The tensor $\mathbf{A}^{(\mathbb{C})}$ is acoustic tensor of classical elasticity. Note that the symmetries of the elasticity tensors $\mathbb{C}$ and $\mathbb{B}$ imply also that $\mathbf{A}^{(\mathbb{C})}$ and $\mathbf{A}^{(\mathbb{B})}$ are symmetric second-order tensors. In addition, it can be readily verified that: $\mathbf{A} = \mathbf{A}^{\mathrm{T}}$ and $\mathbf{\Gamma} = \mathbf{\Gamma}^{\mathrm{T}}$. As it was shown in [1], $\mathbf{A}^{(\mathbb{B})}$ is a singular tensor that always possesses one null eigenvalue corresponding to the eigenvector $\mathbf{n}$, i.e. $\mathbf{A}^{(\mathbb{B})}\mathbf{n} = \mathbf{0}$. The same property is shared by tensor $\mathbf{\Gamma}$. This degeneracy has important implications in the propagation of plane waves. An immediate consequence of the properties of the tensor $\mathbf{\Gamma}$ is that, if $\hbar_{pq}$ is *positive semi-definite*, the two (non-

trivially null) eigenvalues of $\mathbf{\Gamma}$ are always non-negative. Under these circumstances, the tensor $\mathbf{I} + \mathbf{\Gamma}$ is *always positive definite*, and thus invertible. Note that when the Cosserat medium has no micro-inertia ($\mathbf{\Gamma} = \mathbf{0}$) then the acoustic tensor becomes $\mathbb{A} = \mathbf{A}$ [1,3].

For plane waves to propagate a sufficient condition is that the acoustic tensor is positive definite, this implies that the following inequalities must hold [4]

$$\mathbf{p} \cdot \mathbf{A}^{(\mathbb{C})} \mathbf{p} \geq 0, \quad \mathbf{p} \cdot \mathbf{A}^{(\mathbb{B})} \mathbf{p} \geq 0, \quad \mathbf{p} \cdot \hbar \mathbf{p} \geq 0, \qquad \forall \mathbf{p} \neq \mathbf{0} \tag{7}$$

augmented with the condition $\mathbf{p} \cdot \mathbf{A} \mathbf{p} \neq 0$, so that both '$= 0$' cannot simultaneously apply in first two inequalities. In fact, the above conditions imply that $\mathbf{p}$ *cannot* be an eigenvector corresponding to a *null* eigenvalue of both $\mathbf{A}^{(\mathbb{C})}$ and $\mathbf{A}^{(\mathbb{B})}$. The inequalities in (7) constitute the wave propagation (WP) conditions in dynamic constrained Cosserat elasticity with micro-inertia.

The definition of ellipticity (E) is now examined in a way appropriate for the system of the governing partial differential equations in (2). Assuming zero body forces and moments and neglecting inertial effects, the fourth-order governing differential operator $\mathbf{L}$ of constrained Cosserat elasticity assumes the following form

$$\mathrm{L}_{qn}\left(\partial\right) \equiv \mathrm{L}_{qn}^{\mathbb{C}} + \mathrm{L}_{qn}^{\mathbb{B}} = \mathbb{C}_{pqmn} \partial_p \partial_m - \frac{1}{4} e_{pqk} e_{smn} \mathbb{B}_{rkts} \partial_m \partial_p \partial_r \partial_t , \tag{8}$$

with $\mathrm{L}_{qn}^{\mathbb{C}}$ being the second-order (classical lower) part and $\mathrm{L}_{qn}^{\mathbb{B}}$ the fourth-order (higher) part of the operator. It can be shown that the principal part of the symbol of the above operator is degenerate, so that the system of PDEs in couple-stress elasticity is not elliptic in the standard sense [1]. The conditions of ellipticity (E) have been thoroughly investigated in [1, 4] and a procedure to deal with the degeneracy of the principal operator was proposed. The conditions of (E) assume the following form

$$\lambda_2\left(\mathbf{n}\right) \neq 0, \quad \lambda_3\left(\mathbf{n}\right) \neq 0, \quad \tau_\nu = \mathbf{n} \cdot \mathbf{A}^{(\mathbb{C})} \mathbf{n} , \tag{9}$$

where λ_2 and λ_3 are the non-vanishing eigenvalues of $\mathbf{A}^{(\mathbb{B})}$ and $\tau_\nu = \mathbf{n} \cdot \mathbf{A}^{(\mathbb{C})} \mathbf{n}$. The fact that only the conditions (9)$_1$ and (9)$_2$ refer to the Cosserat moduli, whereas condition (9)$_3$ involves the classical (Cauchy) moduli, is attributed to the degeneracy of the principal part of the symbol in couple-stress elasticity. This degeneracy is directly related to the fact that in the constrained Cosserat theory the strain energy depends upon the gradient of the rotation (8 independent components) and not upon the complete gradient of strain (18 independent components).

3 STATIC FOLDING IN A CONSTRAINED COSSERAT MATERIAL

In what follows, the folding of a constrained Cosserat continua is examined under static antiplane strain and plane-strain conditions. The fundamental equations and the conditions of (PD), (WP) and (E) are given in both cases. The route leading to folding is obtained with a perturbation technique, which involves the derivation of a new two-dimensional Green's function for a concentrated force.

3.1 A constrained Cosserat orthotropic material under antiplane strain conditions

When antiplane strain conditions prevail, the displacement field can be expressed in the (x_1, x_2)-plane as: $u_1 = u_2 = 0$ and $u_3 \equiv w(x_1, x_2)$.

Enforcing equilibrium yields a single PDE of the fourth-order for the out-of-plane displacement component

$$Lw + X_3 + \frac{1}{2}\left(\frac{\partial Y_2}{\partial x_1} - \frac{\partial Y_1}{\partial x_2}\right) = 0 \tag{10}$$

where the differential operator L is defined as

$$L \equiv \underbrace{c_{55}\partial_1^2 + c_{44}\partial_2^2}_{L^{cl} \equiv \text{lower (classical) part}} - \frac{1}{4}\underbrace{\left(b_2\partial_1^4 + 2b_0\partial_1^2\partial_2^2 + b_4\partial_2^4\right)}_{L^{cs} \equiv \text{principal part}} \tag{11}$$

with c_{44} and c_{55} being the 'classical' shear moduli characterizing the underlying orthotropic Cauchy material subject to antiplane strain conditions, and (b_1, b_2, b_3, b_4) the couple-stress bending and torsion moduli with the dimension of a force. Moreover, X_3 is the body force component in the out-of-plane direction and (Y_x, Y_y) are the in-plane components of the body couple. Note that neglecting the body force and couple, the equilibrium equation (10) is of the same form as the equation of bending of thin orthotropic plates with *prestress*. In particular, the principal part $L^{cs}w$ is associated with the deflection of the plate, whereas the classical (lower) part $L^{cl}w$ plays the role of the prestress.

The strain energy density W is positive definite (PD) when the material moduli satisfy the following inequalities

$$(\text{PD})^{\mathbb{C}} \Leftrightarrow c_{44} > 0, \ c_{55} > 0, \quad (\text{PD})^{\mathbb{B}} \Leftrightarrow b_1 > 0, \ b_2 > 0, \ b_4 > 0, \ b_2 b_4 - b_3^2 > 0, \tag{12}$$

Further, *sufficient* conditions for waves to propagate in all directions $\mathbf{n}$ and for all wavenumbers in an orthotropic constrained Cosserat material are

$$(\text{WP}) \Leftrightarrow \begin{cases} c_{44} \geq 0, \ c_{55} \geq 0, \\ b_2 \geq 0, \ b_4 \geq 0, \ b_0 \geq -\sqrt{b_2 b_4}, \end{cases} \tag{13}$$

augmented with the condition $A_{33} \neq 0$ where A_{33} is the non-vanishing component of the acoustic tensor (Eq. (5)$_1$) in the antiplane case considered here. In addition, the parameter $b_0 = b_1 - b_3$ is defined in the case of antiplane strain that combines torsional and secondary bending effects.

Finally, the conditions (E) in the antiplane strain case involve only the Cosserat moduli and assume the following form

$$(\text{E}) \Leftrightarrow b_2 b_4 \neq 0, \quad b_0 \neq -\sqrt{b_2 b_4} \tag{14}$$

Note that the (E) conditions for a classical Cauchy orthotropic material are: $c_{55}c_{44} \neq 0$. In what follows, unless otherwise stated, it will be assumed that $c_{44} > 0$ and $b_4 > 0$. Under these circumstances, loss of (E) is attained when either (i.) at the elliptic-imaginary to parabolic (EI/P) boundary, where $b_2 = 0$ and $b_0 > -\sqrt{b_2 b_4}$ or (ii.) at the elliptic-complex to hyperbolic (EC/H) boundary where $b_2 > 0$ and $b_0 = -\sqrt{b_2 b_4}$. In particular, as it will be shown next, at the (EI/P) boundary only one possible discontinuity surface emerges which is aligned parallel to the x_2-axis. On the other hand, at the (EC/H) boundary two discontinuity surfaces are possible. The inclination angle φ (with the x-axis) of the normal to the discontinuity surfaces depends solely upon the ratio b_2/b_4, and can be calculated at the (EC/H) boundary as: $\tan^2 \varphi = \left(b_2/b_4\right)^{1/2}$.

3.1.1 Green's functions for concentrated force and moment

In the case of an out-of-plane concentrated force S the field equation governing antiplane deformations assumes then the following form: $Lw = -S\delta(x)\delta(y)$, where $\delta()$ is the Dirac Delta function. An exact solution is obtained by employing the double exponential Fourier transform in the following form

$$w(x,y) = \frac{S}{4\pi^2} \int_{-\infty}^{\infty} \int_{-\infty}^{\infty} \frac{1}{D(k_1,k_2)} e^{-i(k_1 x + k_2 y)} dk_1 dk_2 \,, \tag{15}$$

where $D(k_1,k_2) = c_{55}k_1^2 + c_{44}k_2^2 + \frac{1}{4}\left(b_2 k_1^4 + 2b_0 k_1^2 k_2^2 + b_4 k_2^4\right)$ is the characteristic polynomial with $\mathbf{k} = (k_1,k_2)$ being the Fourier vector. The inversion integral is evaluated through contour integration and numerical treatment [2]. An analogous procedure is followed for the solution of the concentrated moment problem [2].

There are two cases of loss of (E) in an orthotropic couple-stress material under antiplane strain conditions. The first is at the boundary of the elliptic-imaginary/parabolic regime (EI/P), whereas the second occurs at the boundary of the elliptic-complex/hyperbolic regime (EC/H). It is shown below that in both these cases, the solution produced by the infinite-body antiplane Green's function (15) exhibits weak elastostatic shocks (i.e. finite jump discontinuities in certain components of the deformation gradient). On the other hand, the displacement remains continuous but displays *localized folding*, a phenomenon that cannot be captured within the context of the classical elasticity theory. When the material is perturbed by a concentrated in-plane moment, a faulting instability emerges related with a *finite* discontinuity in the displacement. Finally, note that the Cosserat orthotropic material under antiplane strain conditions is characterized effectively by three dimensionless parameters, namely: $\varepsilon = c_{55}/c_{44}$, $\beta = b_2/b_4$, and $\gamma = b_0/b_4$. A characteristic length ℓ is also defined through the relation $b_4 = 4c_{44}\ell^2$.

3.1.2 Folding and faulting of a Cosserat continuum under antiplane conditions

At the (EI/P) boundary, loss of ellipticity is attained when $\beta = 0$ and $\gamma > 0$, and *single* localized *folding* is formed. On the other hand, at the (EC/H) boundary, loss of ellipticity is attained when $\beta > 0$ and $\gamma = -\sqrt{\beta}$, and *cross localized folding* is formed. Figures 1a and 1b display the single and cross folding of Cosserat material when an antiplane concentrated unit force is applied to an orthotropic material at failure of ellipticity. For the cross folding case, it is observed that when (E) is lost two discontinuity surfaces are created with an inclination of $\varphi = \pm 45^o$ and a double folding emerges along the lines $y = \pm x$. Along these folds the normal derivative of the displacement $\partial_n w$ exhibits a *finite* jump that decays away from the origin. In both cases, although ellipticity fails, the (WP) condition still holds (provided that $c_{44} > 0$ and $c_{55} > 0$), so that the Green's function (15) can still be obtained.
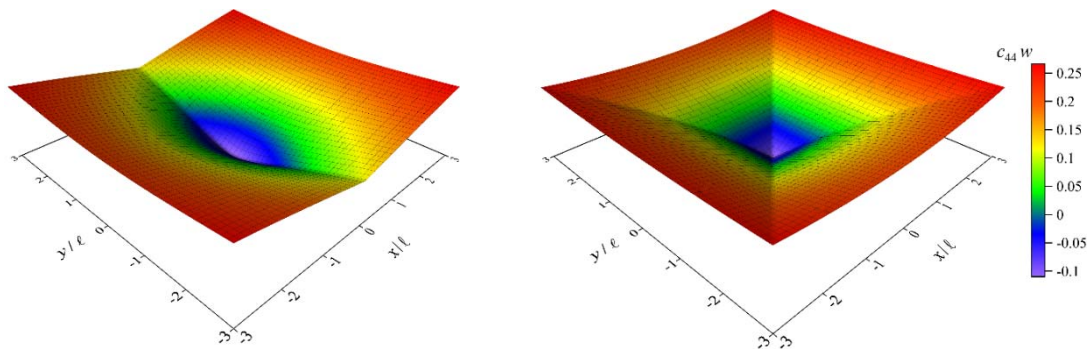
Figure 1: Folding under antiplane strain conditions is evidenced by the dimensionless out-of-plane displacement produced by an antiplane concentrated unit force applied at the origin: (**left**) Single folding emerging at the (EI/P) boundary for an orthotropic material ($\varepsilon = 1/2$, $\beta = 0$, and $\gamma = 1$). (**right**) Cross folding emerging at the (EC/H) boundary for an orthotropic material ($\varepsilon = 1/2$, $\beta = 1$, and $\gamma = -1$).

The application of a concentrated antiplane moment on an extreme Cosserat material at failure of ellipticity yields the emergence of faulting (elastostatic shocks of finite amplitude) in single and cross

geometries. It is worth noting that there is no counterpart of such type of deformation in the classical theory of elasticity. For the case of a concentrated unit moment (assumed parallel to the x_2-axis), the two situations of loss of ellipticity, on the (EI/P) and the (EC/H) boundary are respectively considered in Figs. 2a and 2b, where the dimensionless displacement is plotted. In particular, Fig. 2a shows the formation of *single faulting* along the discontinuity line $x_1 = 0$, at loss of ellipticity at the (EI/P) boundary for an orthotropic Cosserat material. On the other hand, at the (EC/H) boundary, two discontinuity surfaces emerge (Fig. 2b).
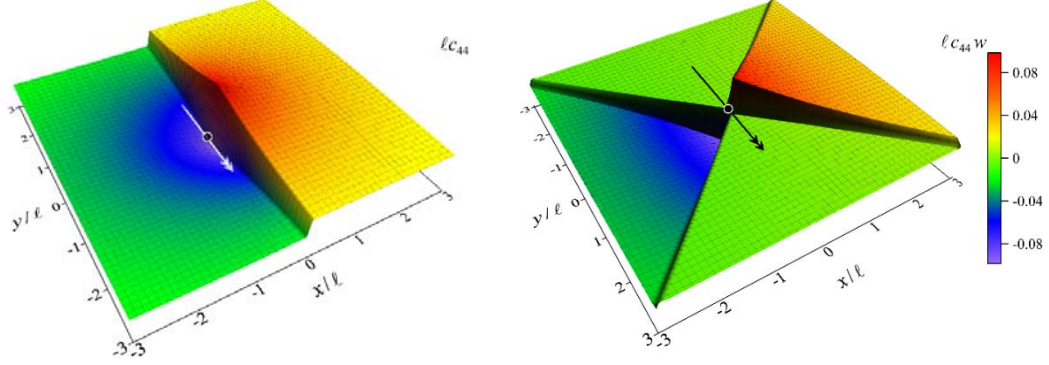
Figure 2: Folding under antiplane strain conditions is evidenced by the dimensionless out-of-plane displacement produced by an antiplane concentrated unit force applied at the origin: (**left**) Single faulting emerging at the (EI/P) boundary for an orthotropic material ($\varepsilon = 1/2$, $\beta = 0$, and $\gamma = 1$). (**right**) Cross faulting emerging at the (EC/H) boundary for an orthotropic material ($\varepsilon = 1/2$, $\beta = 1$, and $\gamma = -1$).

3.2 A constrained Cosserat orthotropic material under plane-strain conditions

When plane strain conditions prevail, the displacement field can be expressed in the (x_1, x_2)-plane as: $u_1 \equiv u_1(x_1, x_2)$ and $u_2 \equiv u_2(x_1, x_2)$, while the out-of-plane component of the displacement is null.

Enforcing equilibrium yields a coupled system of PDEs of the fourth-order for the in-plane displacement vector $\mathbf{u} = (u_1, u_2)$, which can be concisely written as: $\mathbf{L}\mathbf{u} + \mathbf{F} = \mathbf{0}$, where the matrix differential operator is defined as $\mathbf{L} = \mathbf{L}^C + \mathbf{L}^P$ where

$$\mathbf{L}^C = \begin{bmatrix} c_{11}\partial_1^2 + c_{66}\partial_2^2 & (c_{12} + c_{66})\partial_1\partial_2 \\ (c_{12} + c_{66})\partial_1\partial_2 & c_{66}\partial_1^2 + c_{22}\partial_2^2 \end{bmatrix}, \qquad \mathbf{L}^P = (\eta_1\partial_1^2 + \eta_2\partial_2^2)\begin{bmatrix} -\partial_2^2 & \partial_1\partial_2 \\ \partial_1\partial_2 & -\partial_1^2 \end{bmatrix}, \tag{16}$$

with c_{11}, c_{12}, c_{22}, and c_{66} being the 'classical' moduli characterizing the underlying orthotropic Cauchy material subject to plane-strain conditions, and η_1, η_2 the couple-stress bending moduli with the dimension of a force. Moreover, $\mathbf{L}^P$ is the principal fourth order operator, $\mathbf{L}^C$ the lower-order classical elasticity operator, and $\mathbf{F}$ is a generalized force [3].

The strain energy density is positive definite (PD) when the material moduli satisfy the following inequalities

$$(\text{PD})^C \Leftrightarrow c_{11} > 0, \ c_{22} > 0, \ -\sqrt{c_{11}c_{22}} < c_{12} < \sqrt{c_{11}c_{22}}, \ c_{66} > 0, \quad (\text{PD})^B \Leftrightarrow \eta_1 > 0, \ \eta_2 > 0 \tag{17}$$

Further, *sufficient* conditions for waves to propagate in all directions $\mathbf{n}$ and for all wavenumbers in an orthotropic constrained Cosserat material are

$$(\text{WP}) \Leftrightarrow \begin{cases} c_{11} > 0, \ c_{22} > 0 \\ -2c_{66} - \sqrt{c_{11}c_{22}} < c_{12} \leq \sqrt{c_{11}c_{22}}, \end{cases} \quad \text{and} \quad \begin{cases} \eta_1 \geq 0, \ \eta_2 \geq 0, \ \eta_1 + \eta_2 \neq 0, \text{ and } c_{66} > 0 \\ \text{or} \\ \eta_1 > 0, \ \eta_2 > 0, \text{ and } c_{66} \geq 0 \end{cases} \quad (18)$$

Note that when $c_{12} = \sqrt{c_{11}c_{22}}$ or $c_{66} = 0$ with all the other strict inequalities satisfied in Eq. (18), (PD) and (SE) are lost simultaneously, but waves can still propagate. Therefore (SE) is only a sufficient condition for wave propagation in a constrained Cosserat material. The (WP) condition plays a major role for the derivation of the infinite body Green's functions. In what follows it will always be assumed that the (WP) conditions hold always for the constrained Cosserat material.

Finally, the conditions (E) in the plane-strain case involve only the Cosserat moduli and assume the following form

$$(\text{E}) \Leftrightarrow c_{11}c_{22} \neq 0, \ c_{12} \neq -2c_{66} - \sqrt{c_{11}c_{22}}, \qquad \eta_1\eta_2 \neq 0 \qquad (19)$$

Note that the (E) conditions for a classical Cauchy orthotropic material are given by Eqs. (19)$_1$, (19)$_2$ augmented by the relations $c_{66} \neq 0$ and $c_{12} \neq \sqrt{c_{11}c_{22}}$.

In what follows, unless otherwise stated, it will be assumed that $c_{22} > 0$ and $\eta_2 > 0$. Under these circumstances, loss of (E) is attained when either $\eta_1 = 0$ or $c_{11} = 0$. In both cases, the conditions of (E), (SE), and (PD) fail simultaneously. The special case where $c_{12} = -2c_{66} - \sqrt{c_{11}c_{22}}$ will not be considered in the present study since (PD) is lost before (SE). It will be shown that when $\eta_1 = 0$, loss of (E) triggers new phenomena such as folding and faulting that cannot be described by the classical theory.

3.2.1 Green's functions for concentrated force and moment

In the case of an in-plane concentrated force $\mathbf{P} = (P_1, P_2)$, the field equations governing plane-strain deformations assume then the following form $\mathbf{L}\mathbf{u} = -\mathbf{P}\delta(x_1)\delta(x_2)$. An exact solution for the displacement field is obtained by employing the double exponential Fourier transform in the following form

$$u_q(\mathbf{x}) = \frac{P_p}{4\pi^2} \int_{-\infty}^{\infty} \int_{-\infty}^{\infty} \frac{C_{pq}(\mathbf{k})}{D(\mathbf{k})} e^{-i\mathbf{k}\cdot\mathbf{x}} \mathrm{d}k_1 \mathrm{d}k_2 \qquad (20)$$

where $C_{pm}(\mathbf{k}) = \mathrm{Cof}\left[A_{pm}(k, \mathbf{n})\right]$ is the cofactor of the acoustic tensor with components

$$C_{11} = c_{66}k_1^2 + c_{22}k_2^2 + k_1^2\left(\eta_1 k_1^2 + \eta_2 k_2^2\right), \quad C_{12} = C_{21} = -k_1 k_2\left(c_{12} + c_{66} - \left(\eta_1 k_1^2 + \eta_2 k_2^2\right)\right)$$

$$C_{22} = c_{11}k_1^2 + c_{66}k_2^2 + k_2^2\left(\eta_1 k_1^2 + \eta_2 k_2^2\right), \qquad (21)$$

and $D(\mathbf{k})$ is the characteristic polynomial identified with the determinant of the acoustic tensor $D(\mathbf{k}) \equiv \det \mathbf{A} = C_{11}C_{22} - C_{12}^2$. The inversion integral is evaluated through contour integration and numerical treatment [3]. An analogous procedure is followed for the solution of the concentrated moment problem [3]. Note that the Cosserat orthotropic material under antiplane strain conditions is characterized effectively by four dimensionless parameters, namely: $\alpha = c_{11}/c_{22}$, $\delta = c_{12}/c_{22}$, $\varepsilon = c_{66}/c_{22}$, $\beta = \eta_1/\eta_2$, and $\eta_2 = c_{22}\ell^2$, where ℓ is the characteristic length.

3.2.2 Folding and faulting of a Cosserat continuum under plane-strain conditions

In the case of an orthotropic couple-stress material under plane-strain conditions, folding and faulting occurs when the ratio $\beta = \eta_1/\eta_2$ tends to zero or to infinity, so that loss of ellipticity (of the Cosserat part of the constitutive tensors) is attained.

Figure 3 depicts the level sets of the dimensionless displacement components produced by a concentrated unit force $\mathbf{P} = (0, -1)$, aligned with the x_2-axis of orthotropy. More specifically, Fig. 3a on the left shows that in a couple-stress material at the failure of ellipticity the normalized vertical displacement becomes piecewise smooth (so that a vertex is displayed) across the discontinuity line $x_1 = 0$. It is worth noting that for the couple-stress material under investigation, both (E) and (PD) are lost simultaneously when $\eta_1 = 0$, but the (WP) condition still holds, so that the Green's function (20) is well defined. In fact, it is rather remarkable that at the failure of (E) the displacement components remain bounded (apart from the origin) even on the line of discontinuity ($x_1 = 0$). On the other hand, Fig. 3a on the right depicts the response of the underlying classical Cauchy material without Cosserat effects which is positive definite (far from ellipticity loss) and, thus, no localization is observed.
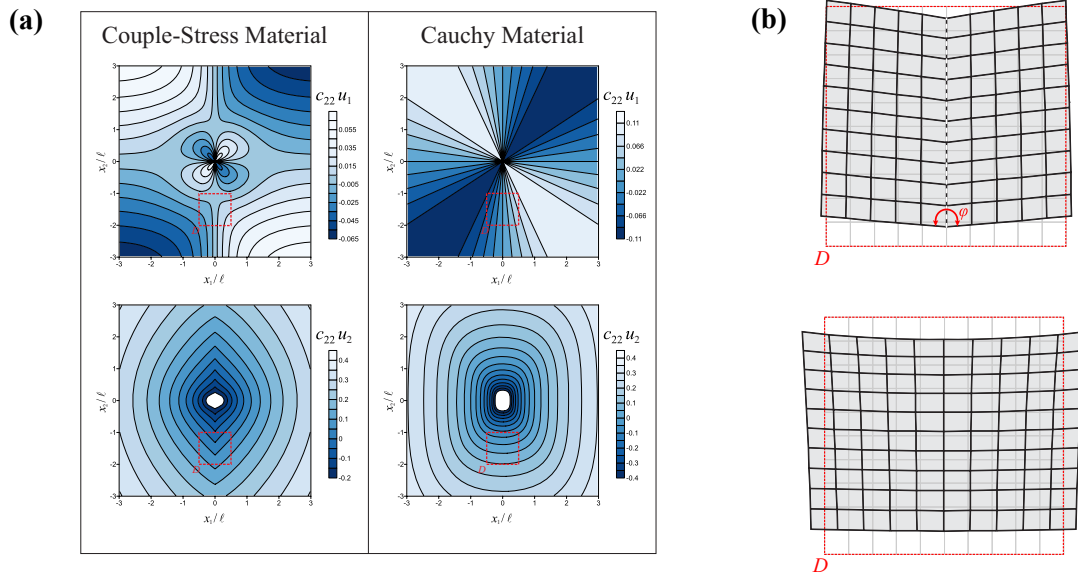
Figure 3: **(a)** Dimensionless level sets of the displacement components $c_{22}u_1$ and $c_{22}u_2$ due to a concentrated unit force acting at the origin of the axes and aligned with the x_2-axis of orthotropy, (*left column*) Couple-stress material at the failure of ellipticity (α=) ($\alpha = 0.5$, $\varepsilon = 0.5$, $\delta = 0.2$, $\beta = 0$), (*right column*) The underlying classical material ($\alpha = 0.5$, $\varepsilon = 0.5$, $\delta = 0.2$) far from ellipticity loss where localization is not observed. **(b)** The actual deformed shape of a rectangular region D referred to the undeformed configuration, (*up*) Folding is clearly visible. (*down*) The underlying classical Cauchy shows a diffused, mild, bending.

The formation of folding in the couple-stress material is more clearly depicted in Fig. 3b, where the actual deformed shape of a rectangular region referred to the undeformed configuration (highlighted with a red rectangle in Fig. 3a) is shown for both the couple-stress and the underlying classical materials. It is observed that the couple-stress material (Fig. 3b, up) folds along the discontinuity line $x_1 = 0$ (white/black dashed line) forming a single (chevron-type) in-plane crease. The lateral sides of the region D remain almost straight and an extremely localized bending (curvature tending to infinity) occurs on the line where the material folds. This situation closely resembles the folding formation in layered rocks and is in marked contrast with the behavior of the underlying classical Cauchy material where all sides of the region D undergo a *small-curvature* diffused bending (Fig. 3b, down).

Figure 4 depicts the level sets of the dimensionless displacement components produced by a concentrated unit out-of-plane moment. In Fig. 4a (left column), it is shown that in a couple-stress material at the failure of ellipticity the vertical displacement becomes discontinuous across the line $x_1 = 0$. On the other hand, in Fig. 4a (right column) the response of a positive definite couple-stress material shows that the displacement field is continuous and, thus, no localization is observed. The formation of faulting is illustrated more clearly in Fig. 4b, where the actual deformed shape of the rectangular region D referred to the undeformed configuration (red rectangle in Fig. 4a), is shown for both the extreme ($\beta = 0$) and non-extreme ($\beta = 0.5$) couple-stress materials. It can be observed that at the failure of ellipticity (Fig. 4b, up) an in-plane slip discontinuity of *finite* width is formed.
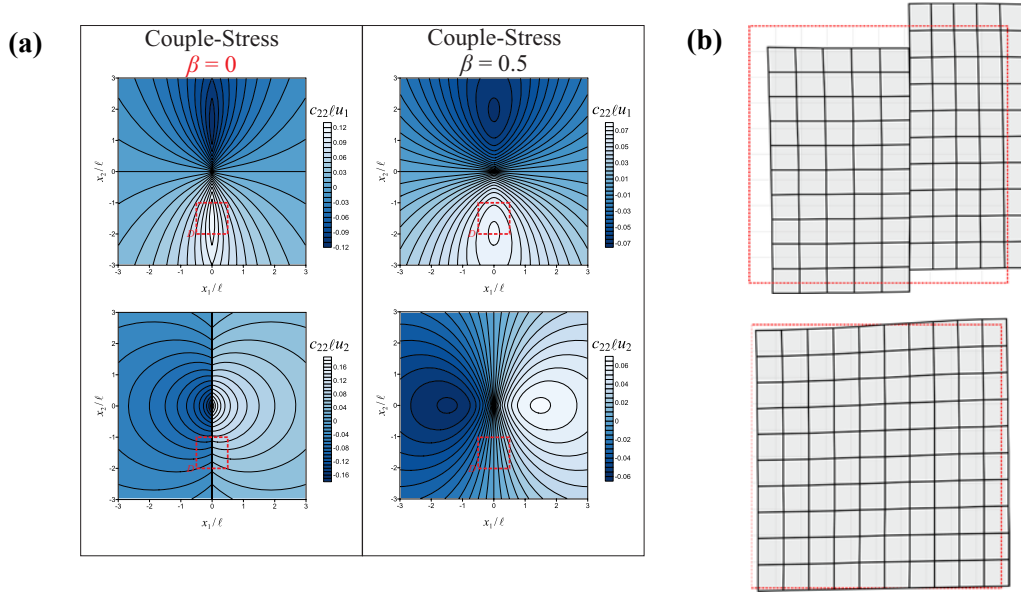
Figure 4: **(a)** Dimensionless level sets of the displacement components $c_{22}\ell u_1$ and $c_{22}\ell u_2$ due to a concentrated unit moment acting at the origin of the axes, (***left column***) Couple-stress material at the failure of ellipticity ($\alpha = 0.5$, $\varepsilon = 0.5$, $\delta = 0.2$, $\beta = 0$) evidences faulting, (***right column***) A couple-stress material far from ellipticity loss ($\alpha = 0.5$, $\varepsilon = 0.5$, $\delta = 0.2$, $\beta = 0.5$). **(b)** The actual deformed shape of a rectangular region D referred to the undeformed configuration, (***up***) Faulting is clearly visible. (***down***) No localization is observed in the positive definite Cosserat material.

4 DYNAMIC FOLDING IN A CONSTRAINED COSSERAT MATERIAL

The time harmonic response of a constrained Cosserat material under antiplane strain conditions is examined revealing the interplay between dynamics and folding mechanisms. Special attention is devoted to the presence of rotational micro-inertia. This feature is explored as connected to pattern formation.

For the time-harmonic case, the out-of-plane displacement assumes the following form: $w(x_1, x_2, t) = w(x_1, x_2)e^{i\omega t}$, and accordingly the equation of motion becomes in the frequency domain

$$\frac{1}{4}\left(b_2 \frac{\partial^4 w}{\partial x_1^4} + 2b_0 \frac{\partial^4 w}{\partial x_1^2 \partial x_2^2} + b_4 \frac{\partial^4 w}{\partial x_2^4} \right) - f_{55} \frac{\partial^2 w}{\partial x_1^2} - f_{44} \frac{\partial^2 w}{\partial x_2^2} - \rho\omega^2 w + X_3 = 0, \tag{22}$$

where $\left(\mathbb{h}_{11}^2, \mathbb{h}_{22}^2 \right)$ are the non-vanishing components of the micro-inertia tensor for an orthotropic Cosserat material under antiplane deformations, and

$$f_{44} = c_{44} - \frac{\rho\omega^2}{12}\hbar_{11}^2, \quad f_{55} = c_{55} - \frac{\rho\omega^2}{12}\hbar_{22}^2 \tag{23}$$

It is important to realize now that, since only the principal 4th order part of the differential operator plays a role in determining the regime classification, the classification of Eq. (22) for the time-harmonic response remains the same as for the static case (see Eq. (14)). It is interesting to observe that the terms f_{44} and f_{55} in Eq. (22) are related to the lower-order part of the differential operator and may change sign according to the values of the micro-inertia parameters for a fixed frequency ω. Indeed, these terms could become negative for high values of micro-inertia parameters, which, in turn, implies that although the equation remains elliptic, the solution would change character. From the viewpoint of plate theory, such a change of sign would correspond to passing from tensile to compressive pre-stress in the x- and y-directions. A time harmonic Green's function for a concentrated force is now evaluated using the same approach as in the static case but now taking into account the contribution of the poles that arise on the real axis due to inertial effects [4]. The inversion integral has the same form as in Eq. (15) but the characteristic polynomial is now defined as:

$$D\left(k_1, k_2\right) = c_{55}k_1^2 + c_{44}k_2^2 + \frac{1}{4}\left(b_2 k_1^4 + 2b_0 k_1^2 k_2^2 + b_4 k_2^4\right) - \rho\omega^2\left(1 + \frac{\hbar_{22}^2}{12}k_1^2 + \frac{\hbar_{11}^2}{12}k_2^2\right). \tag{24}$$

To characterize the material orthotropy, we introduce additionally the following dimensionless parameters: $\theta = \hbar_{22}/\hbar_{11}$ and $\lambda = \hbar_{11}/\ell$. Moreover, a dimensionless frequency $\omega_d = \omega\ell\rho^{1/2}c_{44}^{-1/2}$ is introduced.

4.1 Dynamics of folding patterns in a Cosserat medium

For zero micro-inertia ($\hbar_{11} = \hbar_{22} = 0$) folding is observed at the (EI/P) boundary where loss of ellipticity is attained for $\beta = 0$ and $\gamma > 0$, and at the (EC/H) boundary where loss of ellipticity is attained when $\beta > 0$ and $\gamma = -\sqrt{\beta}$. Figure 5, illustrates the formation of a localized single folding (left) and cross folding (right) due to a harmonic concentrated out-of-plane unit force applied at the origin at a normalized frequency $\omega_d = 1$. Only the real part of the dimensionless out-of-plane displacement is shown.
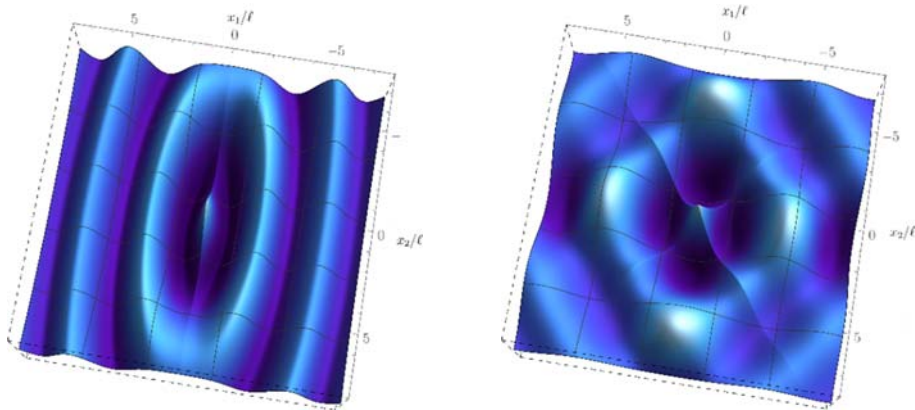
Figure 5: Dynamic response of an extreme orthotropic material without micro-inertia at (**left**) the (EI/P) boundary of (E) loss ($\beta = 0$, $\gamma = 0.25$, $\varepsilon = 0.25$) and (**right**) the (EC/H) boundary of (E) loss ($\beta = 0.5$, $\gamma = -\sqrt{0.5}$ $\varepsilon = 0.25$). Only the real part of the dimensionless out-of-plane displacement is shown as produced by an antiplane concentrated time-harmonic force at the dimensionless frequency $\omega_d = 1$.

The role of micro-inertia is now investigated now as connected to the formation of folding patterns. The behavior of the solution depends strongly upon the terms f_{44} and f_{55} which may change sign according to the magnitude of the micro-inertia parameters.

For single folding emerging at the (EI/P) boundary of loss of (E), two special cases are considered highlighting the effects of micro-inertia, namely, (case a) $f_{44} > 0$, $f_{55} > 0$ and (case b) $f_{44} > 0$, $f_{55} < 0$. Fig. 6 on the left, shows that as the micro-inertia parameters increase, the wavelength of the disturbance decreases significantly as compared to a Cosserat medium without micro-inertia (see Fig.5a). Moreover, the wave fronts become now parallel to the discontinuity line $x_1 = 0$. Further increase of the micro-inertia parameters results in $f_{55} < 0$ and the response to the perturbation changes qualitatively. Indeed, it is shown in Fig. 6 on the right that the disturbance corresponds to a mode of rapidly decaying oscillations in the direction normal to the discontinuity line.
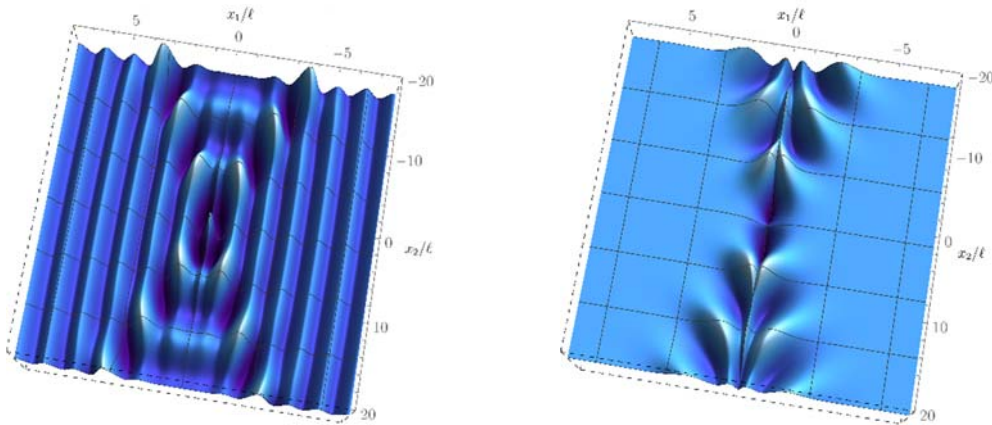
Figure 6: Single folding of an extreme orthotropic material with micro-inertia at the (EI/P) boundary of (E) loss with ($\beta = 0$, $\gamma = 0.25$, $\varepsilon = 0.25$, $\lambda = 1$) (left) Case (a) - $\theta = 0.9\sqrt{3}$ (right) Case (b) - $\theta = 1.1\sqrt{3}$. Only the real part of the dimensionless out-of-plane displacement is shown as produced by an antiplane concentrated time-harmonic force at the dimensionless frequency $\omega_d = 1$. Note that for case (a) the disturbance degenerates into waves propagating only parallel to the folding line ($x_1 = 0$), while for case (b) the disturbance rapidly decays in the x_1 direction, but propagates along the discontinuity line $x_1 = 0$, thus showing an example of a folding wave.
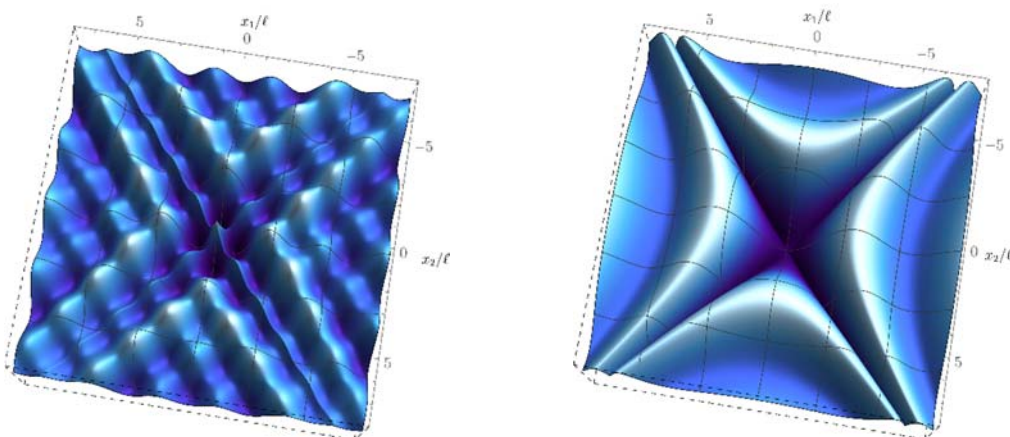
Figure 7: Cross folding of an extreme orthotropic material with micro-inertia at the (EH/C) boundary of (E) loss with ($\beta = 0.5$, $\gamma = -\sqrt{0.5}$ $\varepsilon = 0.25$, $\theta = 0.5$) (left) Case (a) - $\lambda = 1.8\sqrt{3}$ (right) Case (b) - $\lambda = 2.2\sqrt{3}$. Only the real part of the dimensionless out-of-plane displacement is shown as produced by an antiplane concentrated time-harmonic force at the dimensionless frequency $\omega_d = 1$.

For cross folding emerging at the (EH/C) boundary of loss of (E), two special cases are considered highlighting the effects of micro-inertia, namely, (case a) $f_{44} > 0$, $f_{55} > 0$ and (case b) $f_{44} < 0$, $f_{55} < 0$. Fig. 7 illustrates the influence of micro-inertia in the formation of cross folding. As in the case of single folding, it is observed that the wavelength of the disturbance decreases significantly as $\lambda \to 2\sqrt{3}$ (this special value corresponds to the case where $f_{44} = f_{55} = 0$ at $\omega_d = 1$) compared with the respective result for a Cosserat medium with null micro-inertia (Fig. 6 on the right). In addition, the disturbance is produced by the superposition of two wave fronts parallel to the discontinuity lines inclined at $\varphi = 40^o$ in this case that propagate with decreasing amplitude. For $\lambda > 2\sqrt{3}$ the disturbance becomes confined in a zone close to the lines of discontinuity and decays quickly away from them.

5   CONCLUSIONS

Generalized continua, and particularly constrained Cosserat materials, can be designed to possess extreme (near a failure of ellipticity) orthotropy properties and in this way to model folding in a three-dimensional solid. This is impossible within the realm of Cauchy elastic materials. Following this approach, folding, which is a narrow zone of highly localized bending, spontaneously emerges as a deformation pattern occurring in a strongly anisotropic solid. The results of the presented study introduce the possibility of exploiting constrained Cosserat solids for propagating waves in materials displaying origami-patterns of deformation.

REFERENCES

[1]   P.A. Gourgiotis and D. Bigoni. Stress channelling in extreme couple-stress materials part I: Strong ellipticity, wave propagation, ellipticity, and discontinuity relations. *Journal of the Mechanics and Physics of Solids*, **88**, 2016, 150–168.

[2]   P.A. Gourgiotis and D. Bigoni. Stress channelling in extreme couple-stress materials part II: Localized folding vs faulting of a continuum in single and cross geometries. *Journal of the Mechanics and Physics of Solids*, **88**, 2016, 169–185.

[3]   D. Bigoni and P.A. Gourgiotis. Folding and faulting of an elastic continuum. *Proceedings of the Royal Society A. Mathematical, Physical and Engineering Sciences* **472**(2187), 2016, 20160018.

[4]   P.A. Gourgiotis and D. Bigoni. The dynamics of folding instability in a constrained Cosserat medium. *Philosophical Transactions of the Royal Society A* **375**(2093), 2017, 20160159.

[5]   R.D. Mindlin, T.F. Tiersten. Effects of couple-stresses in linear elasticity. *Archives for Rational Mechanics and Analysis*, **11**, 1962, 415-448.